Journal of Applied Fluid Mechanics, Vol. 11, No. 1, pp. 233-240, 2018.
Available online at www.jafmonline.net, ISSN 1735-3572, EISSN 1735-3645.
DOI: 10.29252/jafm.11.01.27116

CFD Study on Jet Stirred Oxidation Pond of Absorption Tower in Power Plant

W. Li[1], Y. Yao[1†] and J. Chen[2]

[1] *Institute of Refrigeration and Cryogenics Engineering, Shanghai Jiao Tong University, Shanghai 200240, China*
[2] *Nanjing Vocational Institute of Transport Technology, Nanjing 211188, Jiangsu Province, China*

†*Corresponding Author Email: yeyao10000@sjtu.edu.cn*

(Received August 27, 2016; accepted August 27, 2017)

ABSTRACT

In the paper, the standard *k-ε* model and the SST *k-ω* model were employed to predict the velocity field in the jet mixing tank, and the simulation results were validated by experimental data. It showed that the standard *k-ε* model can predict the velocity field of jet mixing tank more accurately than the SST *k-ω* model. The standard *k-ε* model was applied to investigate the effects of the jet inclination angle (i.e., 0°, 10°, 20°, 30° and 40°) and the jet velocity (i.e., 14, 16, 18 and 20m/s) on the mixing uniformity of the jet mixing oxidation pond. Based on the evaluation criterions: un-precipitated area ratio (*UPAR*) and non-uniform velocity coefficient (*NUVC*) proposed in the paper, when the jet inclination angle and jet velocity are 10° and 18m/s, respectively, the jet mixing effect in the oxidation pond is the best. The study can be helpful for the optimization of the flow field in the jet mixing oxidation pond to improve the desulfurization efficiency.

Keywords: Jet mixing; Fluent; Inclination angle; Jet velocity; Optimization; Oxidation pond.

NOMENCLATURE

C_μ	constant of conservation of momentum	z	dimensionless axial coordinate
C_ε	constants in ε equation		
g	gravitational acceleration	α^*	coefficient of turbulent viscosity
G	generation of turbulence kinetic energy	ε	turbulent energy dissipation rate
k	turbulent kinetic energy	θ	jet inclination angle
p	pressure	μ_{eff}	effective viscosity of slurry
Re_t	turbulent Reynolds number	μ_{mol}	molecular viscosity
S_o	total area of cross section	μ_t	turbulent viscosity
v	kinetic viscosity	ρ	liquid density
S_A	unprecipitated area of cross section	σ	turbulent Prandtl number
t	time	ω	specific dissipation rate
$u_{i,j,k}$	velocities in i, j and k directions	Γ	effective diffusivity
V_{abs}	absolute velocity	Ω	the absolute value of the vorticity

1. INTRODUCTION

The wet desulfurization technology is a major method removing sulfur dioxide from flue gas in thermal power plants due to its high desulfurization efficiency (Wang *et al.* (2009)). In the wet desulfurization process, calcium carbonate slurry in oxidation pond is pumped into adsorption tower and sprayed out to remove sulfur dioxide from the flue gas through reacting with calcium carbonate. To make the calcium carbonate slurry react with sulfur dioxide more fully, it needs to install a mixing system in the oxidation pond. The mechanical mixer with impeller is often used for mixing in the oxidation pond. But, the mechanical mixer is of low mixing efficiency and high energy consumption. In addition, the impeller mixing system has the risk of slurry leakage, which causes high maintenance costs. In contrast, jet mixing system has the advantages of small size, simple structure and low price, and it will be a potential alternative to the impeller mixing

system in the desulfurization system of power plant.

In the jet mixing system, there are many factors affecting the wet desulfurization efficiency. Among these factors the mixing uniformity of the calcium carbonate slurry plays a decisive role. With regard to the jet mixing, there have been many researches. Fossett and Prosser (1949) firstly studied an inclined side-entry jet in a flat-bottomed cylinder tank,. Fox and Gex (1956) extended the investigation of Fossett and Prosser (1949) for laminar and turbulent regimes and compared the mixing using a jet and a propeller. Coldrey (1978) found that the length of the jet path had relation with the jet mixing time and Reynolds number. Hiby and Modigell (1978) studied the flat-bottom vessel with vertical jet mixer. turbulent viscosity. Lehrer (1981) formulated a model for free turbulent jet of miscible fluid of different density. Maruyama *et al.* (1982) used the conductivity method to observe the jet mixing process. Grenville and Tilton (1996, 1997) reported that the mixing time was governed by the energy dissipation rate. In the simulation study aspect, Ranade (1996) used the standard *k–ε* model to predict the flow field and mixing time. Unger *et al.* (1998) concluded that jet mixing time would become shorter if the jet mixing tank was asymmetric. Jayanti (2001) showed that the key factor of reducing mixing time was to minimize or eliminate dead zones in the reactor by employing CFD. Rahimi and Parvareh (2005) used standard, RNG and realizable models to predict the jet mixing time and the RNG *k–ε* model showed the most convincing results among the other models.

From the above literatures, it can be noticed that the effects of parameters on jet mixing time and the correlations between them have been intensively focused on. However, little literature has been found about the mixing uniformity and its influencing factors on jet mixing tank. In order to improve the desulfurization efficiency, it is very necessary to study the most important factors (jet inclination angle and jet velocity) which affect the mixing uniformity and determine their optimal values.

The objectives of this study are to validate the turbulence models which can be used for the optimal design of the jet mixing oxidation pond with the CFD technology.

2. NUMERICAL METHOD

The standard *k-ε* model is the most widely used model in industrial applications, whose parameters have been validated by a lot of experiments. It has proper accuracies and good stabilities for the majority of flow conditions. The SST *k-ω* model applies more stable low Reynolds number equations to the region near the wall, so it can predict flow field more accurate in viscous sub-layer. And it also contains sub-models about compressibility effect, transition flow and shear flow correction. Therefore, it can simulate the flow with inverse pressure gradient better than other models and is widely used in the field of pneumatic and rotating machinery. In the jet outlet, there may occur shear flow between the flow throughout the jet and the flow in the tank. Considering the standard *k-ε* model can has proper accuracy in the majority of flow conditions, the standard *k-ε* model and SST *k-ω* model are applied to predict the jet mixing flow field.

The Navier-Stokes equations and standard *k-ε* and SST *k-ω* equations (Launder and Spalding (1972)) are used as the governing equations. The effect of heat transfer on the flow field is neglected.

Mass conservation equation

$$\frac{\partial u_i}{\partial x_i}+\frac{\partial u_j}{\partial x_j}+\frac{\partial u_k}{\partial x_k}=0 \tag{1}$$

where x_i, x_j and x_k represent x, y and z coordinates, respectively; u_i, u_j and u_k are velocity components in x_i, x_j and x_k directions (m/s), respectively.

Momentum conservation equation

$$\frac{\partial}{\partial x_j}\left(\rho u_i u_j\right)=\frac{\partial}{\partial x_j}\left[\mu_{eff}\left(\frac{\partial u_i}{\partial x_j}+\frac{\partial u_j}{\partial x_i}\right)-\frac{2}{3}\mu_{eff}\frac{\partial u_k}{\partial x_k}\right]-\frac{\partial p}{\partial x_i} \tag{2}$$

where, ρ is the density of fluid (kg/m^3); p represents pressure (Pa); μ_{eff} is the effective viscosity of fluid.

$$\mu_{eff}=\mu_{mol}+\rho C_\mu\frac{k^2}{\varepsilon} \tag{3}$$

where μ_{mol} is the molecular viscosity (m^2/s); C_μ is a constant of the standard *k-ε* model; k is the turbulence kinetic energy (m^2/s^2); ε is the dissipation rate (m^2/s^3).

Standard k and ε equations

$$\frac{\partial}{\partial t}(\rho k)+\frac{\partial}{\partial x_i}(\rho k u_i)=\frac{\partial}{\partial x_j}\left[\left(\mu+\frac{\mu_t}{\sigma_t}\right)\frac{\partial k}{\partial x_j}\right]+G_k-\rho\varepsilon \tag{4}$$

$$\frac{\partial}{\partial t}(\rho\varepsilon)+\frac{\partial}{\partial x_i}(\rho\varepsilon u_i)=\frac{\partial}{\partial x_j}\left[\left(\mu+\frac{\mu_t}{\sigma_\varepsilon}\right)\frac{\partial\varepsilon}{\partial x_j}\right]+\frac{C_{1\varepsilon}\varepsilon}{k}G_k-C_{2\varepsilon}\rho\frac{\varepsilon^2}{k} \tag{5}$$

In Eq.(4) and Eq.(5), G_k represents generation term of k; μ_t is the turbulent viscosity; σ_k, σ_ε, $C_{1\varepsilon}$ and $C_{2\varepsilon}$ are constants which are 1.0, 1.3, 1.44 and 1.92, respectively.

$$G_k=\mu_t\left(\frac{\partial u_i}{\partial x_j}+\frac{\partial u_j}{\partial x_i}\right)\frac{\partial u_i}{\partial x_j} \tag{6}$$

$$\mu_t=\rho C_\mu\frac{k^2}{\varepsilon} \tag{7}$$

where C_μ is 0.09.

SST k and ω equations Menter (1994)

$$\frac{\partial(\rho k)}{\partial t}=\tau_{ij}\frac{\partial u_i}{\partial x_j}-\beta^*\rho\omega k+\frac{\partial}{\partial x_j}\left[(\mu+\sigma_k\mu_t)\frac{\partial k}{\partial x_j}\right] \tag{8}$$

Table 1 Instruments and equipment in the experimental study

Name	Number	Basic Information	Type/Manufacturer
Centrifugal pump	1	Rated flow: 21m3/h; Lift: 24m	JYWQ20/Hangzhou Kaifeng Company, China
Electronic flowmeter	1	Measuring range: 0-1.5L/s; Measuring error: ±1%	Engelmann 8078/ Engelmann Sensor GmbH, Germany
Jets	3	Inner diameter: 10mm; Length:10mm	Hollow-cone spray/ Shanghai Watchman Company, China
Pressure gauge	3	Measuring range: 0-200KPa; Measuring error: ±1KPa	Hangzhou Tiankang instrument co. Ltd, China
PIV system	1		TSI Company, America

$$\frac{\partial(\rho\omega)}{\partial t}=\frac{\gamma}{v_t}\tau_{ij}\frac{\partial u_i}{\partial x_j}-\beta\rho\omega^2+\frac{\partial}{\partial x_j}\left[(\mu+\sigma_\omega\mu_t)\frac{\partial\omega}{\partial x_j}\right]$$

$$+2(1-F_1)\frac{\rho\sigma_{\omega2}}{\omega}\frac{\partial k}{\partial x_j}\frac{\partial\omega}{\partial x_j} \tag{9}$$

In Eq. (9), F_1 is mixed function, which is defined by

$$F_1=\tanh\left(\arg_1^4\right) \tag{10}$$

$$\arg_1=\min\left[\max\left(\frac{\sqrt{k}}{0.09\omega d},\frac{500v}{d^2\omega}\right),\frac{4\rho\sigma_{\omega2}k}{CD_{k\omega}d^2}\right] \tag{11}$$

where d is the distance to the next surface; $CD_{k\omega}$ is the positive portion of the cross-diffusion term of Eq. (9)

$$CD_{k\omega}=\max\left(2\rho\sigma_{\omega2}\frac{1}{\omega}\frac{\partial k}{\partial x_j}\frac{\partial\omega}{\partial x_j},10^{-20}\right) \tag{12}$$

The eddy viscosity μ_t is defined as

$$\mu_t=\frac{\rho a_1 k}{\max(a_1\omega,\Omega F_2)} \tag{13}$$

where Ω is the absolute value of the vorticity; F_2 is defined by

$$F_2=\tanh\left(\arg_2^2\right) \tag{14}$$

$$\arg_2=\max\left(2\frac{\sqrt{k}}{\beta^*\omega d},\frac{500v}{d^2\omega}\right) \tag{15}$$

β^* and a_1 are 0.09 and 0.31, respectively.

3. EXPERIMENTAL

3.1 Experimental Set-Up

Figure1. shows the pictures of the jet mixing experimental rig. The whole experimental rig is mainly comprised of transparent cylindrical tank, PIV measurement system, centrifugal pump, electronic flowmeter and pressure gauge. The height and diameter of the tank are 800mm and 250mm, respectively. As shown in Fig.2, three hollow-cone spray jets are installed at the height of 290mm and radius of 85mm. The velocity field of shooting area is 175×130mm. The position of laser light sheet through two nozzles and the PIV system records velocity of the cross section.

Fig. 1. Photographs of jet mixing experimental rig.

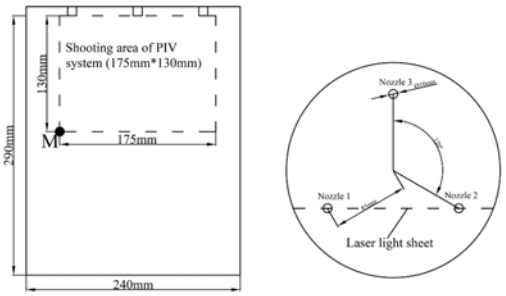

Fig. 2. The illustrations of the shooting and the nozzle positions in the experimental rig.

The main experimental steps in this article are as follows. Distilled water was added into the experimental rig until the liquid height reached 620mm. Then the centrifugal pump was turned on and adjusted to the water flow rate of 1.95m3/h. When the flow was stable, crystal balls (Particle size range:1-5um) were added into the distilled water. The main role of the crystal balls are tracer particles, which move along the water flow. The camera of PIV system took 15 pictures per second to record the positions of the crystal balls in every picture. By analyzing the positions of crystal balls in different pictures of different times, the velocity in flow field could be determined. The pictures of the shooting area must be clear and velocity values of 24 verification points were sort out to compare the simulation results. The coordinates of the 24 verification points are listed in Table 2, and M was set to be the original point.

Table 2 The coordinates of the verification points

(14.5,113.5)	(43.5,113.5)	(72.5,113.5)	(101.5,113.5)	(130.5,113.5)	(159.5,113.5)
(14.5,80.8)	(43.5, 80.8)	(72.5, 80.8)	(101.5, 80.8)	(130.5, 80.8)	(159.5, 80.8)
(14.5,48.5)	(43.5, 48.5)	(72.5, 48.5)	(101.5, 48.5)	(130.5, 48.5)	(159.5, 48.5)
(14.5,16.2)	(43.5, 16.2)	(72.5, 16.2)	(101.5, 16.2)	(130.5, 16.2)	(159.5, 16.2)

4. CFD MODELING

The mesh of the jet mixing experimental rig was generated by the mess generation code (ICEM CFD). The O-Grid scheme was adopted to enhance the quality of the mesh, which is shown in Fig.3. The SIMPLE algorithm, Pressure-based, steady solver was used in the model. The second order upwind difference scheme was applied to the pressure and momentum term, and the first order upwind was used in the standard *k-ε* and the SST *k-ω* transport equations. The boundary condition of nozzle was velocity-inlet, and the condition of wall was set to be adiabatic and nonslip boundary. Grid independence was carried out with 1392513, 1711915 and 1951563 hexahedral cells of the whole computational domain. The difference of the velocities of the 24 verification points for the three computational domains with different grids were less than 1%. In order to reduce the computational time and improve the calculation accuracy, the computational domain with 1711915 hexahedral cells was chosen.

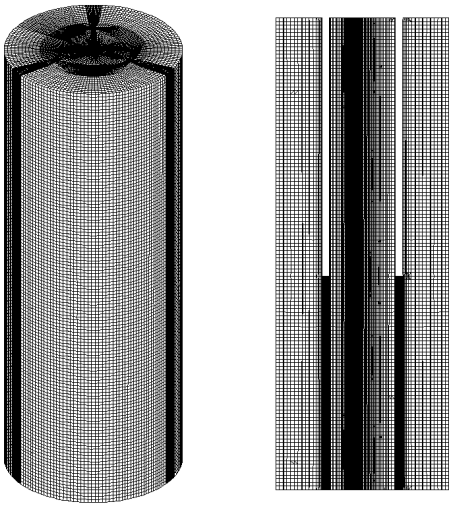

Fig. 3. Mesh of the experimental jet mixing tank cross-section of laser light sheet.

Figure4 shows the velocity contours of the experiment, the standard *k-ε* model and the SST *k-ω* model of M regime. Fig.5 shows the relative errors between the experiment and the simulation results. It can be seen that the velocities of the simulation results are obviously lower than the experimental data, and the deviations of the SST k-ω model compared with the experimental data are larger than that of the standard k-ε model. The mean relative error of the standard k-ε model is shown as 19%, and that of the SST k-ω model is 63%. It indicates that the standard k-ε model is more suitable for studying the jet mixing systems in the oxidation pond of absorption tower than the SST k-ω model.

5. JET INCLINATION ANGLE AND VELOCITY OPTIMIZATION

5.1 Evaluation Criterion of Jet Mixing

As shown in Fig.6, the jet inclination angle is between the jet incident direction and the gravity direction. In this section, two evaluation criterions are proposed to evaluate the effects of the jet inclination angle and the jet velocity on the mixing uniformity.

The un-precipitated area ratio *(UPAR)* is ratio of the area (S_O) where velocity is greater than critical precipitated velocity to the total area (S_A), which is defined by the following equation:

$$UPAR = \frac{S_O}{S_A} \tag{16}$$

where S_o is the area in which fluid velocity is larger than the critical precipitation velocity (m^2), S_A is the total area (m^2).

The *UPAR* cannot be determined by the original grid nodes because the grids of the cross section are unstructured and uneven. It needs to be meshed again. Fig.7 shows the schematic diagram of how to mesh the area again. Assuming that there are four nodes (A, B, C and D) in the new grid, and the mean velocity (V_L) of the grid is calculated as below:

$$V_L = \left(V_A + V_B + V_C + V_D\right)/4 \tag{17}$$

The experimental results manifest when the flow velocity is below 0.2m/s, there will be precipitation, and hence the critical precipitated velocity is set to be 0.2m/s.

The second criterion is non-uniform velocity coefficient (*NUVC*), which represents the degree of deviation between measured velocity and the average velocity of the cross section.

$$NUVC = \sqrt{\frac{1}{n}\left(\sum_{i=1}^{n} V_{abs,i}^2\right) - \left[\frac{\sum_{i=1}^{n} V_{abs,i}}{n}\right]} \tag{18}$$

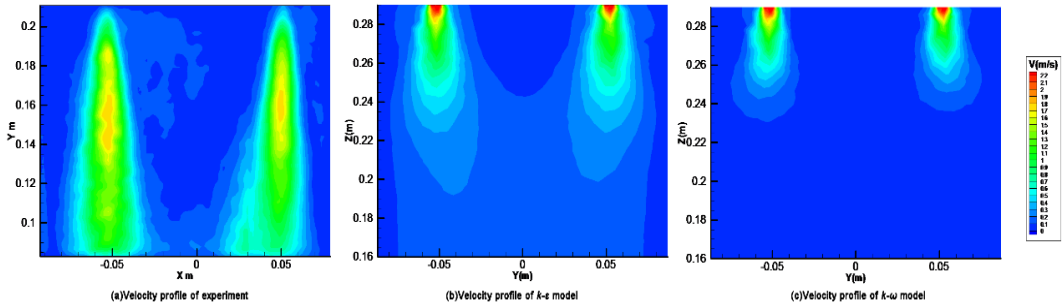

Fig. 4. Velocity contours of (a) experiment, (b) standard *k-ε* and (c) SST *k-ω* model.

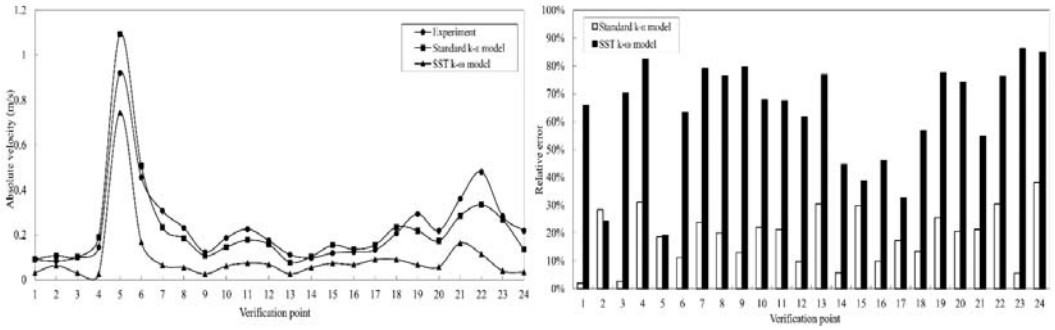

Fig. 5. Comparisons of the absolute velocities and relative errors between the experimental data and simulation results of standard *k-ε* model and the SST *k-ω* model.

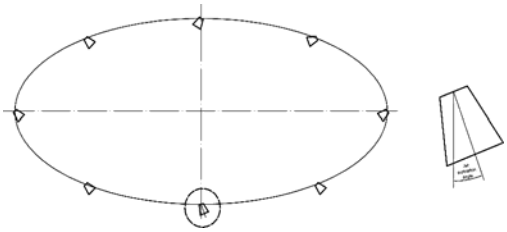

Fig. 6. The schematic diagram of jet inclination angle.

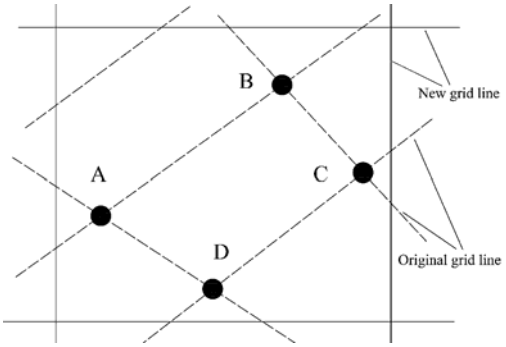

Fig. 7. Schematic diagram of the newly structured grids.

Where V_{abs} is the absolute velocity; n is number of the nodes in the cross section. The mixing uniformity is positively proportional to *UPAR* and inversely proportional to *NUVC*.

5.2 Case Study

Figure8 shows the schematic diagram and mesh of oxidation pond of diameter of 17m.

According to the above results, the standard *k-ε* model can be well applied to predict the velocity field of the oxidation pond. The velocity field of cross section with height of 0.1m is used to investigate the mixing uniformity of the oxidation pond. There are 14 nozzles in the pond, and volume flow rate of every nozzle is 150 m^3/h. The volume of three circulation outlet is 11000 m^3/h. The density of the slurry is 1151 kg/m^3, and the temperature is 50 □, and the viscosity is 0.003Pa·s.

The variations of *UPAR* and *NUVC* of the cross section is illustrated in Fig. 9. As shown in Fig.9 (a), (b) and (c), in the beginning, *UPAR* increases sharply with increasing of the jet inclination angle. It peaks when the jet inclination angle is around 10° and then it decreases sharply. From Fig.9 (d), the *UPAR* decreases to minimum with jet inclination angle of 30° and then inversely increases again from 30° to 40°. The reason of the difference from Fig.9 (a), (b) and (c) is that the areas affected by different jets are overlapped. In the areas directly affected by multiple jets, the mixing uniformity is further improved. Another possible reason is that the whole kinetic energy of the flow field increases with the increasing of jet velocity. From Fig.10 (d), it can be seen that the affected areas of 40° are larger than that of 30°, which can also indicate the variation of the *UPAR* with jet velocity of 20m/s.

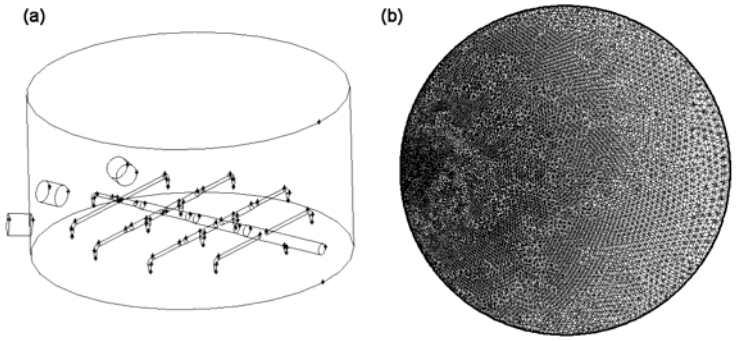

Fig. 8. The schematic diagram of the (a) oxidation pond with diameter of 17m and the (b) mesh of cross section of height of 0.1m.

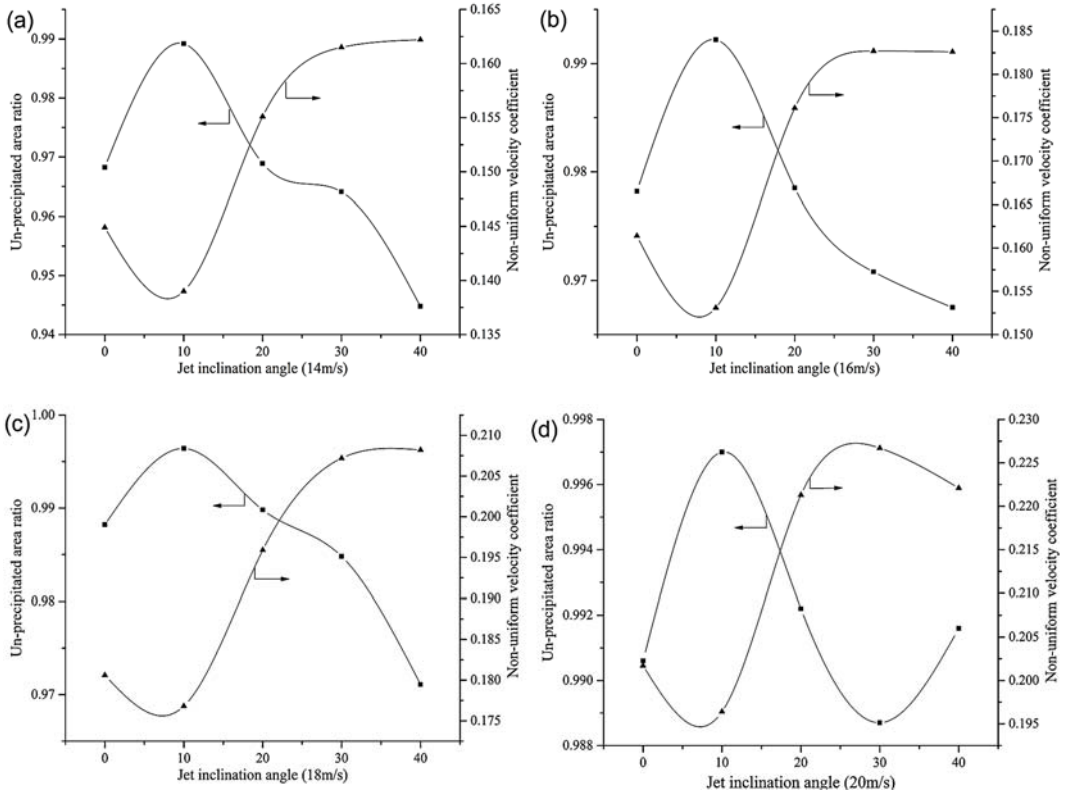

Fig. 9. Variations of *UPAR* and *NUCV* in jet inclination angles (i.e., 0°, 10°, 20°, 30° and 40°) and jet velocities: (a) Jet velocity=14m/s, (b) jet velocity=16m/s, (c) jet velocity=18m/s, and (d) jet velocity=20m/s.

In Fig.9 (a), (b) and (c), the *NUVC* firstly decreases with the jet inclination increasing from 0° to near 8°, and then it begins to increase as the jet inclination increases from 10° to 25°. However, the *NUVC* hardly changes within the range from 30° to 40° in the jet inclination for the case of Fig.9 (a), (b) and (c), and this is different from the case of Fig.9 (d) in which the *NUVC* decreases as the jet inclination increases from 30° to 40°. It can be noticed that the variations of *UPAR* is opposite to *NUVC*, which indicates that the *UPAR* is related to the *NUVC*.

Figure11 shows the variations of *UPAR* and *NUVC* at different jet velocities and jet inclination angles. It can be seen that the *UPAR* reaches maximum when the jet inclination angle is around 10°. When the jet inclination angle remains 10° and the jet velocity changes from 14m/s to 18m/s, the *UPAR* increases obviously, but when jet velocity increases from 18m/s to 20m/s, there is only slight change of the *UPAR*. When the jet velocity is 18m/s, the *UPAR* reaches 0.996. In such case, it can be considered the whole velocity field of the cross section is under precipitation conditions.

As seen from Fig.11 (b), the lowest value of *NUVC* occurs at the jet inclination angle of around 10°. And when the jet inclination angle is 10°, the *NUVC* increases linearly from 0.177 to 0.196 with the jet velocity increasing from 14m/s to 20m/s. Since the

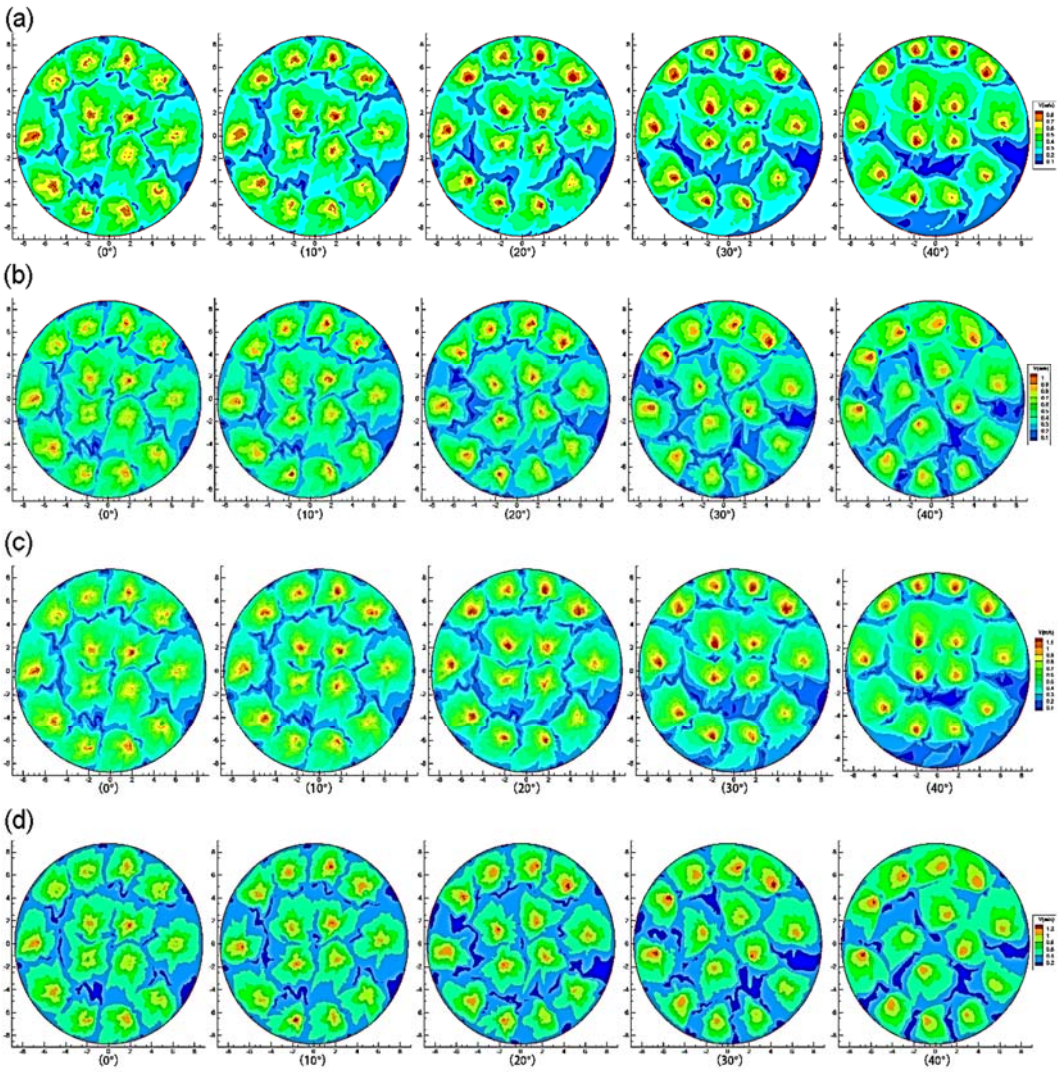

Fig. 10. Velocity contours at different jet inclination angles (i.e., 0°, 10°, 20°, 30° and 40°) and jet velocities ((a) 14m/s, (b) 16m/s, (c) 18m/s and (d) 20m/s).

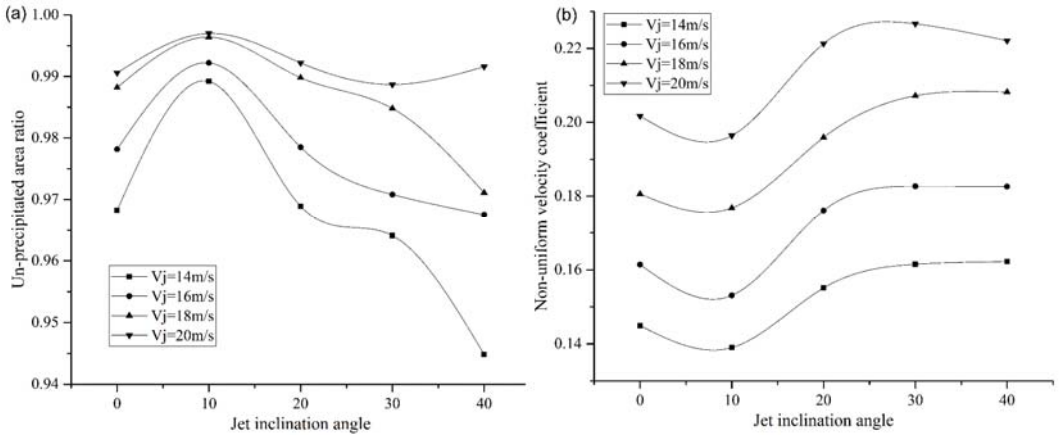

Fig. 11. Variations of (a) *UPAR* and (b) *NUVC* in different jet inclination angles (i.e., 0°, 10°, 20°, 30° and 40°) and jet velocities (i.e., 14m/s, 16m/s, 18m/s and 20m/s).

NUVC is inversely proportional to the mixing uniformity, the higher the jet velocity is, the worse the mixing uniformity will become. In summary, for this case study, the best mixing uniformity and the highest desulfurization efficiency can be achieved at the jet inclination angle of 10° and the jet velocity of 18m/s.

5. CONCLUSION

In this paper, the standard *k-ε* model and the SST *k-ω* model were employed to predict the velocity field of the jet mixing experimental rig and validated by experimental data. The results showed that the standard *k-ε* model could predict the jet mixing velocity field more accurately than the SST *k-ω* model. Then the standard *k-ε* model was used to investigate the effects of jet inclination angle (i.e., 0°, 10°, 20°, 30° and 40°) and jet velocity (i.e., 14, 16, 18 and 20m/s) on the mixing uniformity of the oxidation pond with diameter of 17m. The simulation results showed that when the jet inclination angle and the jet velocity were 18m/s and 10° respectively, the degree of mixing uniformity in the oxidation pond was the highest and the maximum desulfurization efficiency could be achieved. The work is of great importance to the optimal design of the jet mixing oxidation pond with the CFD technology.

ACKNOWLEDGEMENTS

This work was supported by Zhejiang Feida Desulfurization Engineering Co., Ltd.

REFERENCES

Coldrey, P. (1978). paper to IChemE Course. *University of Bradford, England*.

Fossett, H. and L. Prosser (1949). The application of free jets to the mixing of fluids in bulk. *Proceedings of the Institution of Mechanical Engineers, 160*(1), 224-232.

Fox, E. and V. Gex (1956). Single□phase blending of liquids. *AIChE Journal, 2*(4), 539-544.

Grenville and Tilton. (1996). A new theory improves the correlation of blend time data from turbulent jet mixed vessels. *Chemical engineering research & design 74*(3), 390-396.

Grenville and Tilton. (1997). *Turbulence or flow as a predictor of blend time in turbulent jet mixed vessels.* Paper presented at the Proceedings of the North European Conference on Mixing.

Hiby, J. and M. Modigell (1978). Experiments on jet agitation 6th CHISA Congress: Prague.

Jayanti, S. (2001). Hydrodynamics of jet mixing in vessels. *Chemical Engineering Science, 56*(1), 193-210.

Launder, B. and D. Spalding (1972). Lectures in mathematical models of turbulence, 1972: Academic Press, London, England.

Lehrer, I. (1981). New model for free turbulent jets of miscible fluids of different density and a jet mixing time criterion. *Transactions of the Institution of Chemical Engineers 59*(4), 247-252.

Maruyama, T. and Y. Ban and T. Mizushina (1982). Jet mixing of fluids in tanks. *Journal of Chemical Engineering of Japan 15*(5), 342-348.

Menter, F. R. (1994). Two-equation eddy-viscosity turbulence models for engineering applications. *AIAA journal 32*(8), 1598-1605.

Rahimi, M. and A. Parvareh (2005). Experimental and CFD investigation on mixing by a jet in a semi-industrial stirred tank. *Chemical Engineering Journal 115*(1), 85-92.

Ranade, V. (1996). Towards better mixing protocols by designing spatially periodic flows: The case of a jet mixer. *Chemical Engineering Science 51*(11), 2637-2642.

Unger, D. R. and F. J. Muzzio and R. S. Brodkey (1998). Experimental and numerical characterization of viscous flow and mixing in an impinging jet contactor. *The Canadian journal of chemical engineering 76*(3), 546-555.

Wang, X. f. and L. Liu and Y. j. Ruan and G. q. Zhang (2009). Summarize present situation on application of our country burns coal haze desulphurization technology. *Coal 18*(9), 4-7.